BULLETIN OF THE POLISH ACADEMY OF SCIENCES
TECHNICAL SCIENCES, Vol. 68, No. 5, 2020
DOI: 10.24425/bpasts.2020.134666

Estimation of the force causing the levitation of the starting trolley of the unmanned aerial vehicle

A.SIBILSKA-MROZIEWICZ[1], E. ŁADYŻYŃSKA-KOZDRAŚ[1*], K. FALKOWSKI[2], and K. SIBILSKI[3]

[1] Warsaw University of Technology, Faculty of Mechatronics, ul. Boboli 8, 02-525 Warsaw, Poland
[2] Military University of Technology, Mechatronics and Aerospace Faculty, ul. Kaliskiego 2, 00-908 Warsaw, Poland
[3] Air Force Institute of Technology, ul. Księcia Bolesława 6, 01-494 Warsaw, Poland

Abstract. The work discusses numerical and experimental researches, which are focused on developing a coherent model of magnetic interactions causing the levitation of the starting trolley of the unmanned aerial vehicle (UAV) catapult. The starting trolley is levitating over the catapult's tracks, which generate the magnetic field. The levitation is made possible by the diamagnetic properties of high-temperature superconductors, placed in supports of the starting trolley. The introduction of the article briefly analyzes the catapult structure. Next, it explains the nature of associated with the Meissner and flux pinning effect magnetic interactions which causes the levitation phenomenon. The paper presents the results of numerical analysis of the magnetic field, generated by the catapult's tracks arranged in two configurations: a "chessboard" and a "gutter" pattern. The numerical model was solved, using the finite element method. Parameterization of the numerical model was made based on the measurements of the magnetic field, generated by a single magnet.

Key words: magnetic field, passive magnetic suspension, high-temperature superconductors, levitation force, magnetic UAV catapult.

1. Introduction

Unmanned aerial vehicles (UAV) are becoming increasingly popular in both military and civilian applications. As predicted by experts, they have great potential in applications such as public UAV safety or the commercial market. These systems could serve as high altitude long endurance persistent surveillance and reconnaissance platforms or communications relay point [1]. The potential civilian application is the use of these vehicles to determine the shoreline of natural watercourses [2]. They are well-suited for image-collection operations, such as tracking and searching for objects [3].

To meet the needs of the modern market, UAV designers must solve several technical problems related to the critical aspects of UAV service. UAV safe take-off and landing procedures are undoubtedly one of these issues.

The launch of most UAV requires the operation of separate devices, known as launchers or catapults. Currently, rocket systems, spring, pneumatic or hydraulic launchers are most often used for take-off [4]. A promising alternative is the use of magnetic interactions in the design of the launcher.

1.1. Prototype of the magnetic UAV catapult. The innovative prototype of the magnetic UAV catapult, using passive suspension with superconductors, was created as part of the European GABRIEL [5–7] project. Part of this project was the development of small-scale test bench demonstrating the possibility of MAGLEV system for safe aircraft take-off and landing. This testbench (catapult) was described in the ICAS paper [8], and it is shown in Fig. 1. In the previous works, the authors of this publication focused on the development of the mathematical model describing dynamics of levitation sledge and aircraft taking-off from this sledge [9]. Paper [10] described models of forces acting on this system. One of the possible applications of such levitation launching system has been described in [11].

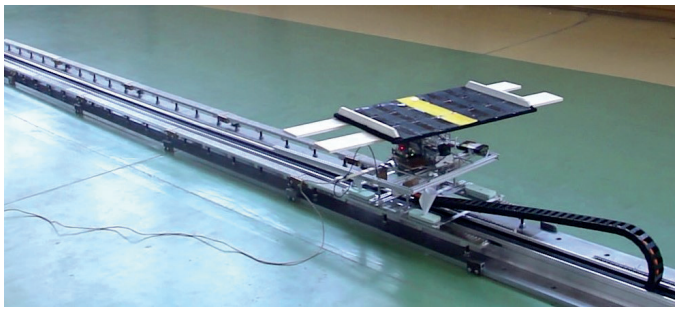

Fig. 1. The prototype of magnetic UAV catapult constructed within GABRIEL project

The catapult consists of rails and a starting trolley levitating above the tracks. Catapult rails are built of neodymium magnets rails generating the magnetic field. The levitation is made possible by the diamagnetic properties of high-temperature superconductors YBCO, placed in supports of the starting trolley. During the take-off, the aircraft is attached to a platform, inte-

*e-mail: e.ladyzynska@mchtr.pw.edu.pl

Manuscript submitted 2019-12-18, revised 2020-06-05, initially accepted for publication 2020-06-20, published in October 2020

grated with the starting trolley. The longitudinal movement of the trolley is generated by a magnetic linear motor. The trolley is made of a duralumin, nonmagnetic frame. Integrated with the starting trolley part of the catapult's suspension system consists of four containers, fastened to the bottom of the frame corners. Containers are made of the material with high thermal insulation properties. Each container contains four YBCO high-temperature superconductors with a critical temperature of 92 [K]. These superconductors have a shape of cylinders with a diameter of 21 mm and a height of 8 mm (Fig. 2). The starting trolley hovers over the tracks, due to the levitation force, that operates between the YBCO, hidden in trolley's supports and the magnetic field, generated by permanent magnets, glued on the launcher rails.

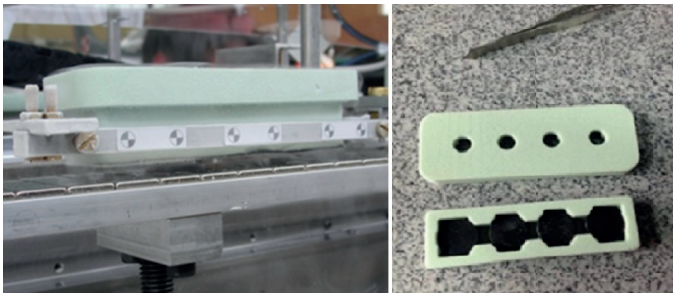

Fig. 2. Container with high-temperature superconductors

The launching route of the catapult consists of two parallel lines of rails, attached to the device base. Catapult's magnetic rails are made of the aluminum beams, to which three rows of magnets are glued. In the track's construction, neodymium magnets with dimensions of $15 \times 15 \times 5$ mm were used. The magnets polarization was towards the smallest dimension – the height.

During the design and assembly of the launchers prototype two arrangements of magnets polarizations were analyzed and examined. The first solution is like a chessboard (configuration a of the Fig. 3) when each edge of the magnet contacts a magnet with the opposite polarization. The configuration in "chessboard" is easy to create. In the second configuration, the columns of magnets have been polarized in opposite directions. Along the rails, the magnets are in contact with magnets with the same polarizations direction, while crosswise – with the opposite (configuration b of the Fig. 3). This arrangement was used in the full-size launchers prototype GABRIEL.

As seen in Fig. 16 b) the magnetic field created above this configuration has a shape of a "gutter". Arrangement of this configuration of magnets was a difficult task, requiring specialized engineering solutions, because there had been a strong repulsive force acting between the magnets with the same polarization.

Described configurations of magnets' polarizations are not the only possibilities. In the Super-Maglev project, magnetic tracks are made of two rows of neodymium magnets, each polarized in a horizontal direction and separated by a layer of ferromagnetic [12]. A similar configuration of magnets was used on the tracks of the Supra-Trans project [13]. The Cobra project

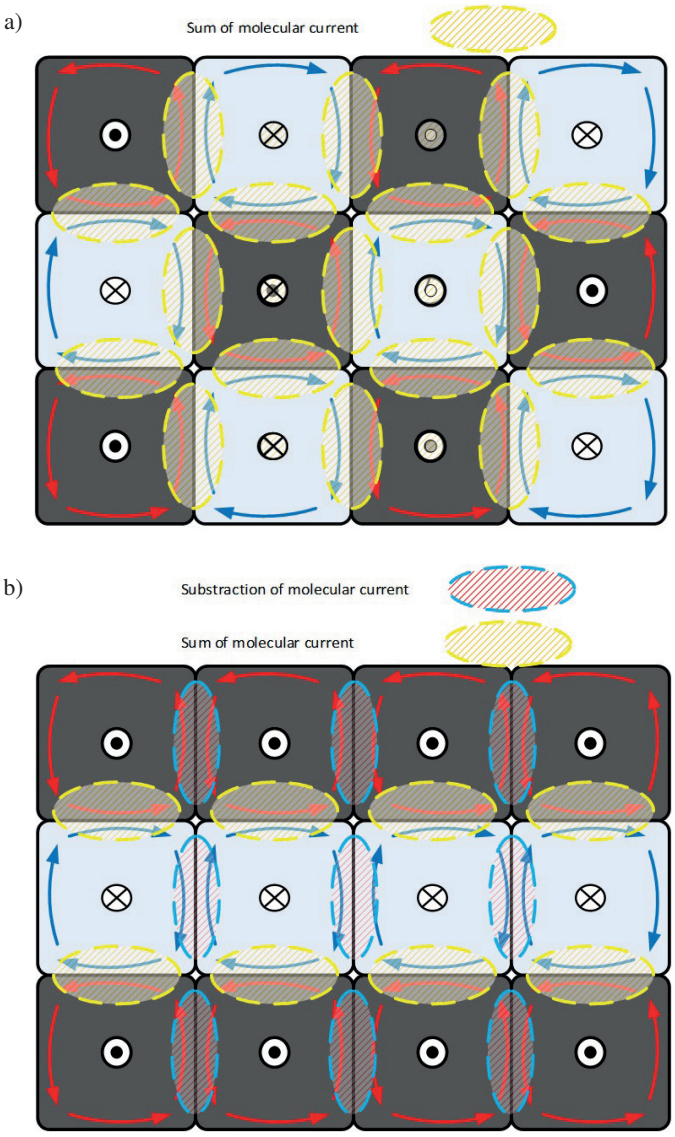

Fig. 3. Two analyzed configurations of magnets polarizations: a) "chessboard" and b) "gutter"

uses 5 rows of neodymium magnets, arranged in the Halbach array [14].

Due to the combined advantages of no-contact friction and self-stable levitation, high temperature superconducting magnetic levitation has significant potential. Currently, work is underway to optimize the configuration of magnets to further improve the performance of such devices [15, 16].

The magnetic force is a result of an interaction between the magnetic flux density $\boldsymbol{B}$ of the magnetic field generated by catapult's rails and electric current induced inside superconductors [17]. The magnetic force generated by surface current $\boldsymbol{K}$ [18]:

$$\boldsymbol{F} = \int (\boldsymbol{K} \times \boldsymbol{B})\, \mathrm{d}a, \tag{1}$$

where: $\mathrm{d}a$ – the element of surface. The cross product in the equation (1) shows that the value of magnetic forces dependent form the orientation of vectors.

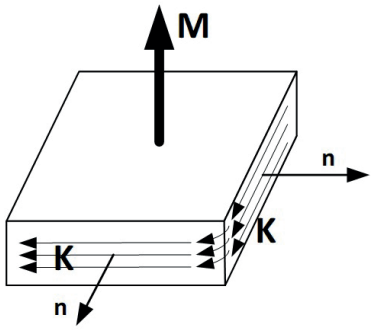

Fig. 4. The surface current in the magnets [18]

The magnetic field in the magnet is generated by the surface current in the active wall of magnets. The surface current is presented in Fig. 4. It is equal [19]:

$$\boldsymbol{K} = \boldsymbol{M} \times \boldsymbol{n} \tag{2}$$

where: $\boldsymbol{n}$ – normal vector and $\boldsymbol{M}$ – magnetization vector. The rectangular magnets from Fig. 4 merge in the array with the orientation of the magnetization as presented in Fig. 5. The next magnets of the array have the opposite direction of the magnetization vector. The surface current in the adjacent active walls of two magnets adds. The result of the summation surface current in the connection wall gives the greater magnetic flux density than the single magnet (Fig. 6 and Fig. 7).

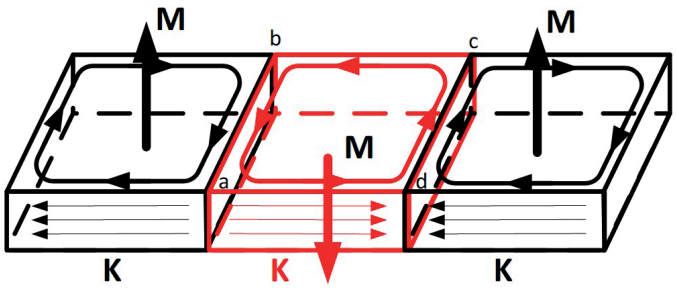

Fig. 5. The magnetization vector in the magnets array [18]

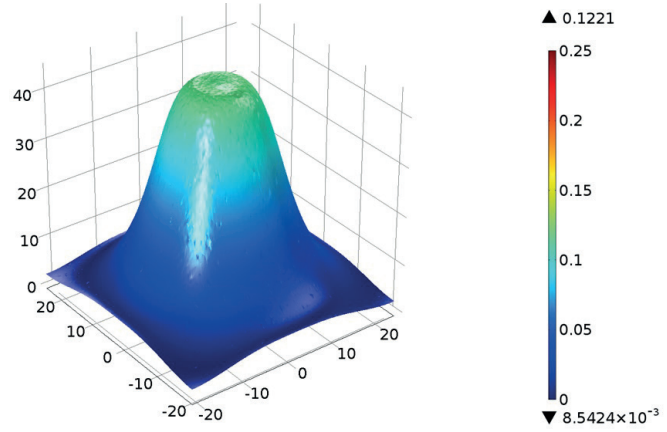

Fig. 6. The magnetic flux density for the magnet (measured 5 mm over the surface) [18]

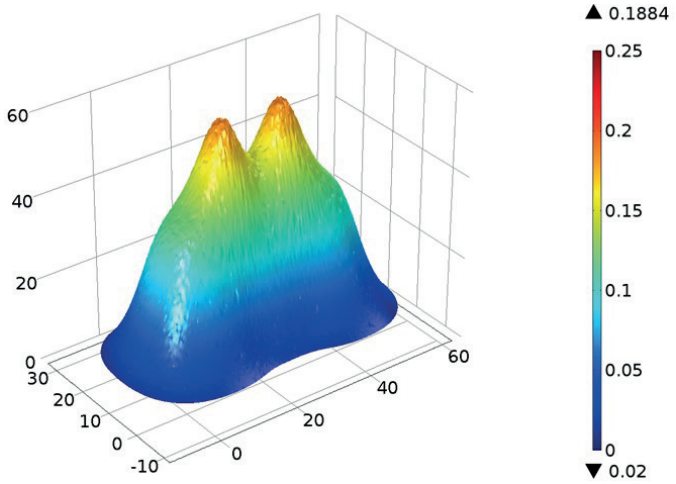

Fig. 7. The magnetic flux density for the array magnets (measured 5 mm over the surface) [18]

The rectangle magnets ensure good adhesion between neighboring magnets in an array. The dimension of magnets will select the configuration of the array (Fig. 3 and Fig. 5). The most important is the width of the central magnet. The relation between the dimensions of central magnet and superconductors strongly influence the levitation [20].

2. The levitation forces

There can be distinguished two types of forces influencing the lift of the starting trolley over the launcher tracks: forces resulting from the Meissner effect and forces and torques associated with the flux trapping phenomenon. The levitation force resulting from the Meissner effect is directed always perpendicular to the tracks and its value, as a function of the levitation gap. The value of the force can be approximated based on experimental investigations [21]. The analysis of lateral movement, when the superconductor moves across an inhomogeneous magnetic field requires considerations of the forces and torques that rotate the superconductor and push it towards the track's center. These interactions result from the phenomenon of the magnetic flux pinning, which is the consequence of the penetration of the magnetic field into the interior of the II type superconductors [22].

An analytical investigation shows that levitation force depends on the magnetic field induction. To investigate the spatial distribution of the vector field of magnetic induction, the numerical model of the magnetic field, generated by the two previously discussed arrangements of magnets – "chessboard" and "gutter" been calculated.

2.1. The levitation force resulting from the Meissner effect.

The value of levitation force depends not only on the intensity of the magnetic field, but also on the shape and size of the superconductor. The result of levitation force, acting on the superconductor placed in the magnetic field is shown in Fig. 8.

Fig. 8. The influence of levitation force on two different superconductors

The levitation force is result of the Meissner effect, described as "pushing" the magnetic field out of the superconductor [17]. The Meissner effect can be explained using the London's equation [23]. The matter "defends" against the change of the magnetic field, inducing in its interior, in precise distance from the surface, the flow of electric charges. The induced current shields the external field and resist to the change in the magnetic field inside the conductor.

In normal conductors the induced current consists of electrons, interacting with the network ions. Collisions of electrons and ions result in energy loss and flow resistance. In the superconductors, the induced current carriers are Cooper pairs [24], which flow inside the material without any resistance. The induced currents change the superconductor into the source of the magnetic field, which magnetization vector is always facing contrary, to the external field. Earnshaw's theorem [25], which dispels the possibility of the stable levitation of the static magnetic systems does not apply to the systems with superconductors. This is because the superconductor magnetization vector is dynamically positioned always opposite to the external magnetic field, which ensures the stability of the levitation system.

2.2. Force and torque resulting from flux pinning effect. If the superconductor was placed in the magnetic field at the time of the transition to the superconducting state, then the magnetic field fluxes, penetrating the bulk's interior were shielded by the vortexes of the superconducting current. As a result, the superconductor itself has a non-zero magnetic moment. The value and orientation of superconductor's magnetic moment depend on the intensity and shape of the external magnetic field at the point of space, occupied by the superconductor at the time of flooding it with liquid nitrogen. This phenomenon is called the flux trapping effect. If the position or orientation of the superconductor, in relation to the magnetic field changes, then the superconductor will be affected by force and torque (as seen in Fig. 9) pushing the superconductor towards the center of the launcher's track.

Fig. 9. The influence of force and torque resulting from flux pinning effect

The phenomenon of flux pinning [26] also occurs spontaneously when high temperature superconductor flooded in zero field moves relative to the magnetic field. Over time, more magnetic fluxes penetrate the interior of the superconductor. The movement of the fluxes pinned inside the superconductor cause the energy dissipation.

As a result of the flux pinning phenomenon superconductors placed inside trolley's supports become magnetized. The advanced mirror image method [27] widely used in modeling of magnetic-superconductor interactions states that levitation force can be described by relation:

$$\boldsymbol{F} = \boldsymbol{m} \cdot \nabla \boldsymbol{B}, \tag{3}$$

where $\boldsymbol{B}$ is the external magnetic field and $\boldsymbol{m}$ is an image of magnetic moment frozen inside superconductor during the moment of state transition.

In a similar fashion, torque, that acts on a superconductor is proportional to the following cross product [28]:

$$\boldsymbol{T} = \boldsymbol{m} \times \boldsymbol{B}, \tag{4}$$

The crucial and not fully established part of describing levitation interactions is the definition of magnetic moment $\boldsymbol{m}$. A review of possible solutions can be found in [29].

As shown by equations the value of force and torque acting on the superconductor due to flux pinning effect depends on three features: the spatial distribution of the magnetic field, generated by magnets placed on the launcher's track; the orientation and position of the superconductor, relative to the magnetic tracks and the value of magnetic field, generated by magnetic fluxes pinned inside the superconductor.

The model of magnetic interactions, resulting from the flux pinning, requires the model of the spatial distribution of the magnetic field over the launcher's tracks. In the performed investigations numerical model of the magnetic field was calculated using the finite element method.

3. Experimental details

In order to calibrate the numerical model of the magnetic field, generated by the launcher tracks, we carried out experiments measuring the magnetic field generated by the single N38 neodymium magnet having dimensions of $15 \times 15 \times 5$ mm. The results of the measurements were compared with the simulations results of the FEM model.

The magnetic field has been measured at the equally spaced points of space, located on three vertical lines over the characteristic points of the magnet: above its middle, above its lateral edge (2.5 mm from the edge) and above its vertex (1.5 mm from two corner edges). The position of selected points is shown in Fig. 10. The experiments were carried out for both poles of the magnet: the north one, for which the sensor indicated positive values, and the southern one, for which the sensor indicated negative values. A detailed description of the test bench and performed measurements have been included in the article [30].

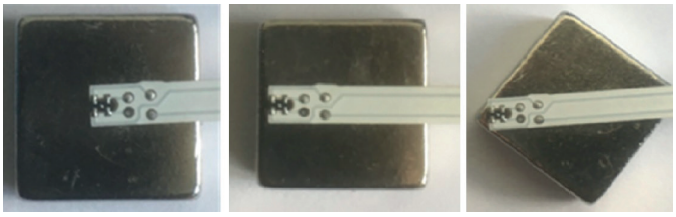

Fig. 10. The measuring points above magnets center, edge and vertex

Figure 11 shows box plots, describing the statistics of magnetic field measurements, as a function of distance. Presented graphs are aggregations of the results of 20 measurements: 5 probe measurement cycles in two directions and for two magnets polarizations.

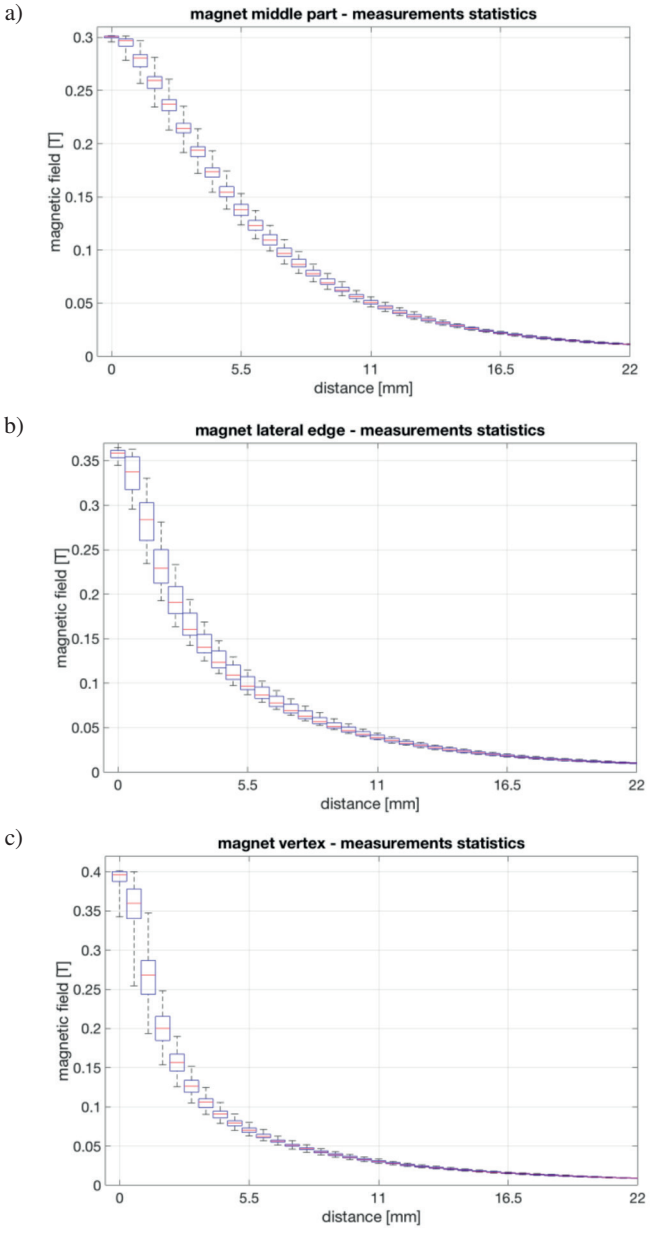

Fig. 11. The statistics of magnetic field measurements above magnet's: a) center, b) edge, c) vertex, as a function of distance

The box plots give information about the average value of measurements and the dispersion of the measurement samples. The height of the box represents the difference between the first (bottom edge) and the third (top edge) quartile of measurements. The red line inside the box represents the average value of the measurements, while the mustache includes the maximum and minimum measured value.

The highest magnetic field value of 0.4 T was measured over the magnet's corner on its surface. A slightly lower value of 0.36 T was measured above the edge of the magnet. The measurements taken above the center of the magnet reached the value of 0.3 T.

4. The numerical model of the magnetic field

The studies of the spatial distribution of the magnetic field generated by rails were based on the numerical model. The numerical model of the vector field of magnetic induction has been calculated using the ANSYS implementing the Final Element Method. The problem was solved using magnetostatic module described by Poisson equation [31]:

$$\Delta \boldsymbol{A} + \mu_0 \boldsymbol{J_M} = \boldsymbol{0}, \tag{5}$$

where $\boldsymbol{A}$ is vector potential of the magnetic, magnetic permeability of vacuum is described by $\mu_0 = 4\pi\ 10^{-7}$ [Tm/A] and $\boldsymbol{J_M}$ [A/m^2] is magnetisation current, which depends on the permanent magnets magnetization:

$$\boldsymbol{J_M} = \nabla \times \boldsymbol{M}. \tag{6}$$

To solve differential equation Dirichlet's boundary conditions were applied to the magnet's surface. The magnetic vector potential is vanishing on the surface surrounding the model at the distance of 15 cm away from the magnets surface.

4.1. Parameters of the numerical model. The launcher's magnetic rails are made of rare earth magnets made of Neodymium, Iron and Boron alloy: $Nd_2Fe_{14}B$. Neodymium magnets are the strongest permanent magnets currently available on the market. Magnet designations range from N35 to N52 and determine the maximum magnetic energy stored inside the magnet. In addition to the maximum magnetic energy density $(B_{H\max})$ and Curie temperature (T_C – the temperature at which the magnet loses its magnetic properties) magnets are characterized by two values: magnetic coercivity (H_C) and remanence (B_r).

Magnetic coercivity describes the value of the external magnetic field, that must be applied to the ferromagnetic to reduce the magnetic residual to zero while the remanence of the ferromagnetic is the value of the magnetic induction, remaining in the material after the removal of the external magnetic field. The launcher tracks were made of N38 neodymium magnets. According to the technical data remanence of magnets varies in the range: 1.22–1.26 T, while their coercivity is over 907 kA/m.

4.2. The numerical model of a single magnet. The numerical model of the magnet and generated magnetic field were calculated using the finite element method. The mesh of the model is shown in Fig. 12. To determine the exact values of parameters of the numerical model, a series of simulations was carried out to study the effect of remanence and coercivity.

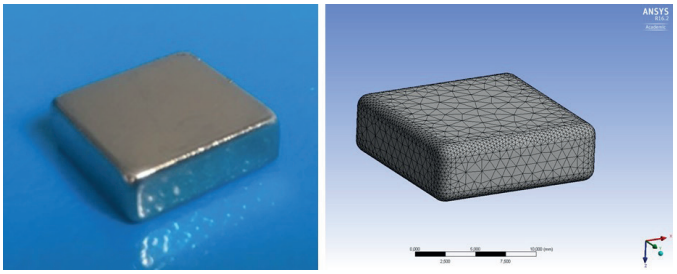

Fig. 12. The modeled neodymium magnet and the finite element mesh

Figure 13 and Table 1 present the results of the simulation, most closely reflecting the actual distribution of the magnetic field. These results were obtained for magnetic coercivity $H_c =$ 900 kA/m and remanence $B_r = 1.22$ T.

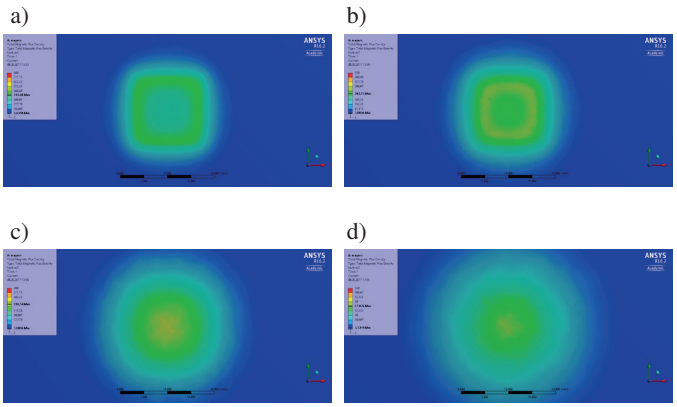

Fig. 13. A model of the magnetic field above a single magnet at the height: a) 1 mm, b) 2 mm, c) 5 mm, d) 10 mm

Table 1
The results of simulations of spatial distribution of the magnetic field, generated by the single magnet

height [mm]	the maximum value of the module of the magnetic induction [mT]	location of the maximum value of the magnetic field
1	350	edge
2	260	edge
5	150	center
10	67	center

Analyzing the results obtained, it can be concluded that the magnetic field decreases faster over the edges and corners of the magnet. The values of the module of the magnetic induction obtained using a numerical model coincide to a large extent with the magnetic field measurements. Both numerical and experimental results indicate that at the lowest distance from the magnet, the largest magnetic field occurs around the corners and edges of the magnet. As the observer moves away from the magnet, the maximum value of the magnetic field is noticed above the center of the magnet.

4.3. The numerical model of a launcher's rails. At the next phase of the research, we calculated the numerical model of the magnetic field, generated by the launcher's tracks consisting of seven rows of magnets arranged in a "chessboard" and "gutter" configuration. The models adopted the value of coercivity and remanence in accordance with the model of a single magnet. In simulations, it was assumed that the magnets are surrounded by air, at a distance of 30 cm around each side of the model. A mesh of finite elements, size 2 mm, was placed on the magnet's surroundings. The magnet models were calculated using a mesh of size 0.5 mm. An inflation algorithm was used in the area of contact between the magnet and the air.

From the results presented in Fig. 14 and Table 2, it can be concluded that below 5 mm, the relative difference between the maximum magnetic field module, generated by the configuration of the "gutter" and "chessboard" is small and does not exceed 10%, while at the height above 5 mm the relative difference is significant and reaches 45%.

Table 2
The results of simulations of spatial distribution of the magnetic field, generated by the launcher's magnetic rails arranged in a "chessboard" and "gutter" configuration

height [mm]	"chessboard"		"gutter"	
	the maximum value of the module of the magnetic induction	location of the maximum	the maximum value of the module of the magnetic induction	location of the maximum
1	698 mT	all joints of magnets	768 mT	joints of magnets columns
2	456 mT	all joints of magnets	516 mT	joints of magnets columns
5	198 mT	evenly distributed	257 mT	near to the rails center
10	78 mT	evenly distributed	112 mT	near to the rails center
15	32 mT	near to the rails corners	59 mT	evenly distributed

Figure 15 and Table 3 describe the distribution of the x, y and z magnetic field components. The z-axis is directed perpendicular to the rails, while the y-axis indicates the longitudinal direction of the launcher. The simulations results show the magnetic field distribution at a height of 2 mm above the rails. The

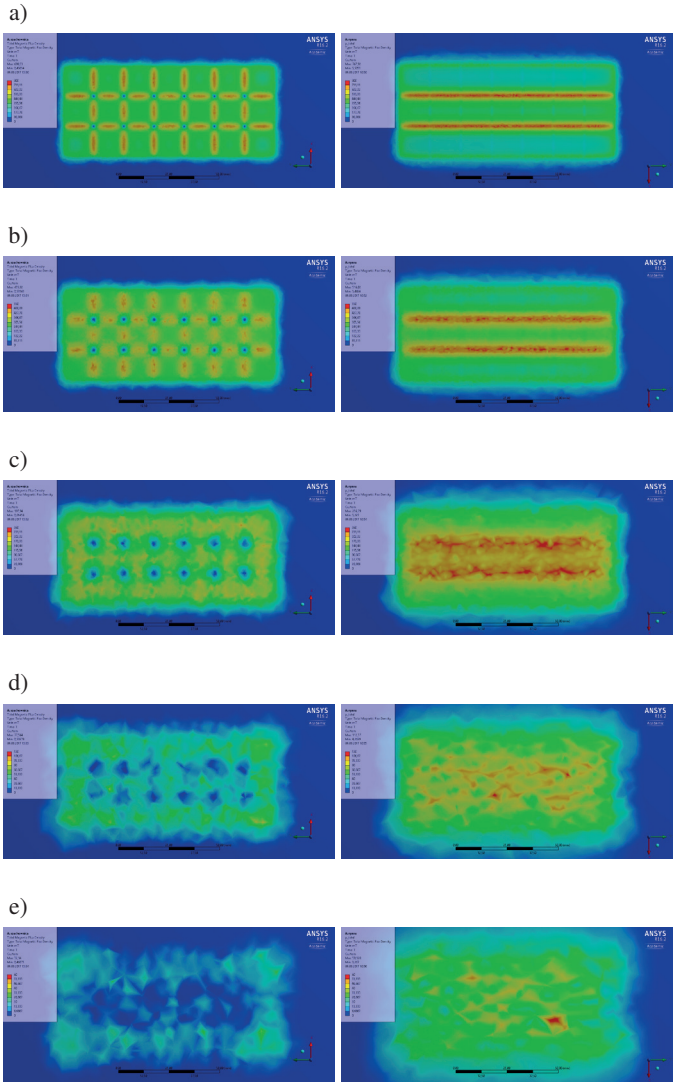

Fig. 14. The magnetic induction module at a height of: a) 1 mm, b) 2 mm, c) 5 mm, d) 10 mm and e) 15 mm above the launcher's magnetic rails arranged in a "chessboard" (results on the left side) and "gutter" (results on the right) configuration

figures on the left side correspond to the configuration of the "chessboard", while on the right – the "gutter".

In the "gutter" configuration, both the magnetic field module and the vertical field component have a higher value at all heights. What is more important, the value and sign of the vertical component of the magnetic field remain uniform along the tracks. It can be concluded that the greater levitation force is exerted on the superconductor, placed in the magnetic field generated by the configuration of the gutter. The *X* component of the magnetic field influences the stabilization of the superconductor's position and pushes it towards the middle of the tracks. The value of the *X* component is larger in the "gutter" configuration and its direction is unchanged along the longitudinal rails line. The *Y* component of the magnetic field slows down the cart's movement. The value of the *Y* component in the chessboard configuration is the same as *X* component and larger than the most "important" *Z* component (determining levitation

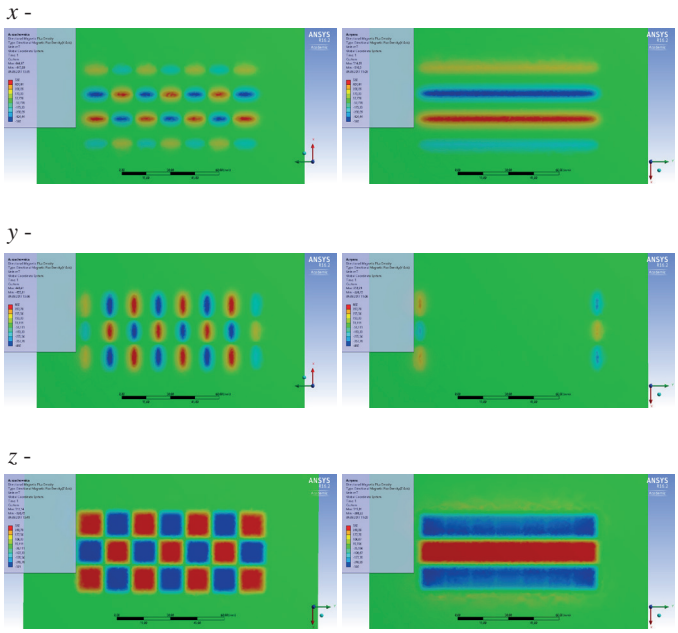

Fig. 15. The *x*-, *y*-, *z*-axis component of the magnetic induction at a height of 2 mm over the track of magnets arranged in a "chessboard" and "gutter"

Table 3
The values of components of the magnetic induction vector of numerical model calculated for the "chessboard" and "gutter" configuration

Component of the magnetic induction vector	"chessboard"		"gutter"	
	the maximum value of the module of the magnetic induction	location of the maximum	the maximum value of the module of the magnetic induction	location of the maximum
x	445 mT	joints between magnets columns	514 mT	joints between magnets columns
y	449 mT	joints between magnet's rows	230 mT	exterior rail's edges
z	312 mT	magnet's interior	315 mT	magnet's interior

force value). The *Y* component in the gutter configuration has negligible value".

Finally, vector representation of the magnetic field induction at different heights over the track, arranged in the gutter configuration was analyzed (Fig. 16).

Analyzing Fig. 16 one can see, that the magnetic field over the rails creates a "gutter" and the gradient of the magnetic field along the track line is equal to zero, so there is no force to inhibit the longitudinal movement of the levitating cart. A non-zero magnetic field gradient across the tracks "pushes" the cart to the rails' center, which significantly affects the stability of the suspension system.

a)

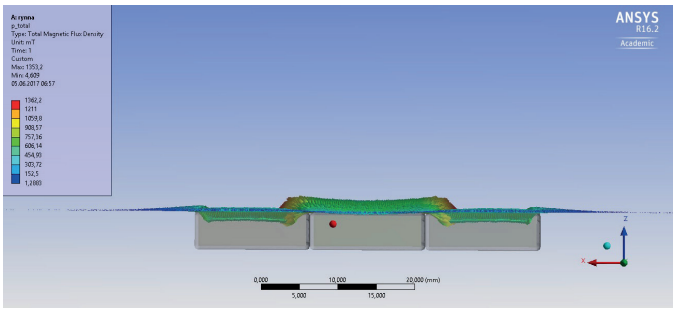

b)

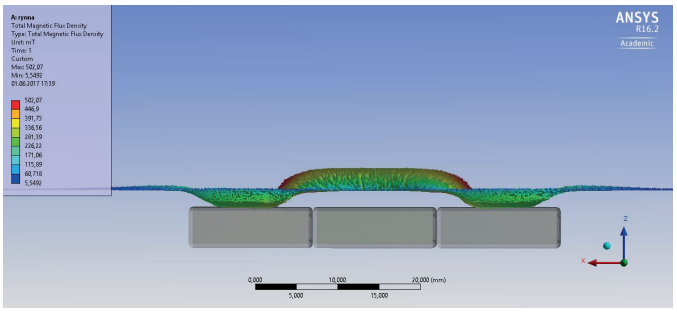

c)

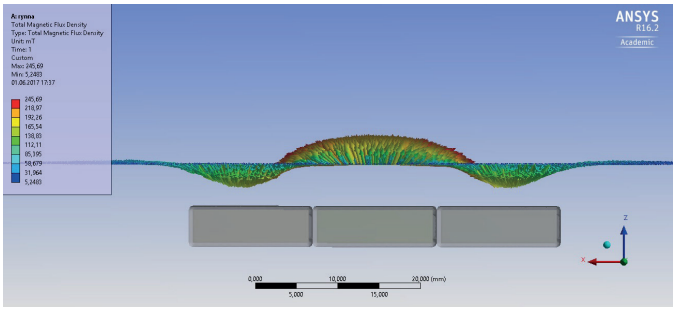

d)

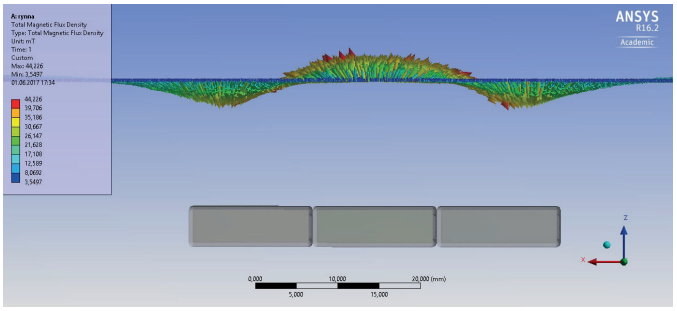

Fig. 16. Vector representation of the magnetic field induction over the track, arranged in the gutter configuration a) directly above the magnet, b) on the height of 2 mm, c) 5 mm, d) 15 mm

5. Conclusions

The developed estimation of the components magnetic force causing the levitation of the starting trolley of the UAV catapult was one of the most difficult elements of analysis of the system's dynamics. Research has shown that the strength of levitation depends on the shape and intensity of the magnetic field, which is correlated with configurations of magnets along the track.

In the configuration of the "gutter", both the magnetic field module and its vertical component have a higher value. In addition, regardless of the height, the value and sign of the vertical magnetic field component remain uniform along the tracks, whereby there is no magnetic force inhibiting longitudinal movement of the trolley. From the presented research results it can also be concluded that in the "gutter", the magnetic field component across the tracks has a higher value. This fact affects the stabilization of the lateral movements of the trolley. The presented facts constitute significant advantages of such magnet's configuration, despite the difficulties with tracks construction, resulting from strong repulsive force acting between the magnets with the same polarization.

From the presented research results it can be concluded that for numerical analysis of the longitudinal movement of the trolley and simulation of the takeoff and landing of the aircraft it is enough to take into account the strength of levitation resulting from the Meissner phenomenon. This allows to assume, that the force of levitation is always directed perpendicular to the tracks.

The performed researches are the basis for numerical simulations of the spatial trajectory of aircraft and trolley movement during take-off and landing procedure. Those simulations should also take into consideration the lateral movements of trolley, influenced by flux pinning effect and non-uniform magnetic field distribution.

Acknowledgements. This study was partially supported by a grant of the Dean of the Faculty of Mechatronics and by a subsidy from financial resources for the maintenance and development of didactic and research potential granted for 2019.

References

[1] Z. Goraj, A. Frydrychewicz, R. Świtkiewicz, B. Hernik, J. Gadomski, T. Goetzendorf-Grabowski, *et al.*, "High altitude long endurance unmanned aerial vehicle of a new generation – A design challenge for a low cost, reliable and high performance aircraft", *Bull. Pol. Ac.: Tech.* 52 (3), 173–194 (2004).

[2] W. Wilkowski, M. Lisowski, M. Wyszyński, and D. Wierzbicki, "The use of unmanned aerial vehicles (drones) to determine the shoreline of natural watercourses", *J. Water Land Dev.* 35, 259–264 (2017).

[3] Z. Kuś, "Analysis of dynamical properties of object tracking system elements", *Bull. Pol. Ac.: Tech.* 64 (3), 479–489 (2016).

[4] M. Sadraey, *Unmanned Aircraft Design: A Review of Fundamentals*, Morgan & Claypool Publishers, 2017.

[5] D. Rohacs and J. Rohacs, "Magnetic levitation assisted aircraft take-off and landing (feasibility study–GABRIEL concept)", *Prog. Aeronaut. Sci.* 85, 33–50 (2016).

[6] J. Rohacs and D. Rohacs, "Problems and Barriers Impeding the Implementation of MagLev Assisted Aircraft Take-Off and Landing Concept", *J. Transp. Technol.* 8 (2), 91–118 (2018).

[7] D. Rohacs, M. Voskuijl and N. Siepenkötter, "Evaluation of landing characteristics achieved by simulations and flight tests on a small-scaled model related to magnetically levitated advanced take-off and landing operations", in *29th Congress of the International Council of the Aeronautical Sciences*, 2014.

[8] K. Sibilski, K. Falkowski, R. Kaleta, E. Ładyżyńska-Kozdraś and A. Sibilska-Mroziewicz, "Development of the Small-Scale Model of Maglev System Assisted Aircraft Safety Take-off and Landing", in *30th Congress of the International Council of the Aeronautical Sciences*, 2016, pp. 25–30.

[9] A. Sibilska-Mroziewicz and E. Ładyżyńska-Kozdraś, "Mathematical Model of Levitating Cart of Magnetic Uav Catapult", *J. Theor. Appl. Mech.* 56 (3), 793–802 (2018).

[10] A. Sibilska-Mroziewicz, E. Ładyżyńska-Kozdraś, and K. Falkowski, "Modelling of Forces Acting on a System of the UAV Launcher, Based on Passive Magnetic Suspensions with Superconductors", *Our Sea* 67 (1), 60–68 (2020).

[11] E. Ładyżyńska-Kozdraś, A. Sibilska-Mroziewicz, S. Czubaj, K. Falkowski, K. Sibilski, and W. Wróblewski, "Take-off and landing magnetic system for UAV carriers", *J. Mar. Eng. Technol.* 16, 298–304 (2017).

[12] J. Wang, S. Wang, Y. Zeng, H. Huang, F. Luo, Z. Xu, *et al.*, "The first man-loading high temperature superconducting maglev test vehicle in the world", *Physica C* 378–381, 809–814 (2002).

[13] L. Schultz, O. de Haas, P. Verges, C. Beyer, S. Rohlig, H. Olsen, *et al*., "Superconductively levitated transport system-the supratrans project", *IEEE Trans. Appl. Supercond.* 15 (2), 2301–2305 (2005).

[14] D. Dias, G. Sotelo, F. Sass, E. Motta, R. de Andrade, and R. Stephan, "Dynamical tests in a linear superconducting magnetic bearing", *Phys. Procedia*, 36, 1049–1054 (2012).

[15] X. Liu, B. Deng, S. Bao, C. Liang, Y. Wan, B. Liu, *et al*., "Magnetic Field Test on an Electromagnetic Turnout Prototype System for High-Tc Superconducting Maglev", *IEEE Trans. Appl. Supercond.* 30 (1), 1–6 (2020).

[16] Z. Deng, W. Zhang, Y. Chen, X. Yang, Ch. Xia, and J. Zheng, "Optimization study of the Halbachpermanent magnetic guideway for hightemperature superconducting magneticlevitation", *Supercond. Sci. Technol*. 33, 034009 (2020).

[17] A. Szewczyk, A. Wiśniewski, R. Puźniak, and H. Szymczak, *Magnetism and superconductivity*, PWN, Warszawa, 2012, [in Polish].

[18] K. Falkowski, *Passive magnetic suspensions*, WAT, Warszawa, 2016, [in Polish].

[19] D.J. Griffiths, *Introduction to Electrodynamics*, PWN, Warszawa, 2005, [in Polish].

[20] Ch. Kimm, *Superconductor Levitation. Concepts and Experiments*, Springer, 2019.

[21] E. Ładyżyńska-Kozdraś and A. Sibilska-Mroziewicz, "Analysis of the Levitation Forces Generated by High-Temperature Superconductors Located within the Magnetic Field of a UAV catapult System", *Problems of Mechatronics. Armament, Aviation, Safety Engineering* 8 (3), 87–94 (2017).

[22] B. Rosenstein and D. Li, "Ginzburg-Landau theory of type ll superconductors in magnetic field", *Rev. Mod. Phys*. 82 (1), 109–168 (2010).

[23] R. Feynman, R. Leighton, and M. Sands, *The Feynman lectures on physics*, vol. III ch. 21, PWN, 1972.

[24] J. Bardeen, L. Cooper, and R. Schrieffer, "Theory of superconductivity", *Physical Review*, 108:1175, 162–164 (1957).

[25] W. Jones, "Earnshaw's theorem and the stability of matter," *Eur. J. Phys.* 1 (2), 85 (1980).

[26] M. McHenry and R. Sutton, "Flux pinning and dissipation in high temperature oxide superconductors", *Prog. Mater. Sci.* 38, 159–310, (1994).

[27] A. Kordyuk, "Magnetic levitation for hard superconductors", *J. Appl. Phys. (Melville, NY, U. S.)*, 83 (1), 610–612 (1998).

[28] F.C. Moon, *Superconducting levitation: Applications to bearings and magnetic transportation*, John Wiley & Sons, 2008.

[29] P. Bernstein and J. Noudem, "Superconducting magnetic levitation: principle, materials, physics and models", *Supercond. Sci. Technol*. 33 (3), 033001 (2020).

[30] E. Ładyżyńska-Kozdraś, A. Sibilska-Mroziewicz, and S.K. Czubaj, "Experimental Measurement of Magnetic Field Generated by Neodymium Magnet", in *Mechatronics 2017: Recent Technological and Scientific Advances*, 2018, vol. 644, pp. 562–570.

[31] Z. Csendes, J. Weiss, and S. Hoole, "Alternative vector potential formulations of 3-D magnetostatic field problems", *IEEE Trans. Magn.* 18 (2), 367–372 (1982).